
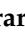




Brief Report

Phenotypic Definition and Genotype-Phenotype Correlates in PMPCA-Related Disease

Valentina Serpieri ^{1,2}, Tommaso Biagini ³, Concetta Mazzotta ¹, Rosa Pasquariello ⁴, Anna Rubegni ^{4,5}, Filippo Santorelli ⁴, Gerardo Ongari ², Silvia Cerri ², Tommaso Mazza ³, Roberta Battini ^{4,5} and Enza Maria Valente ^{1,2,*}

- ¹ Department of Molecular Medicine, University of Pavia, 27100 Pavia, Italy; valentina.serpieri01@universitadipavia.it (V.S.); concetta.mazzotta01@universitadipavia.it (C.M.)
² IRCCS Mondino Foundation, 27100 Pavia, Italy; gerardo.ongari@mondino.it (G.O.); silvia.cerri@mondino.it (S.C.)
³ Bioinformatics Laboratory, IRCCS Casa Sollievo della Sofferenza, 71013 San Giovanni Rotondo, Italy; t.biagini@css-mendel.it (T.B.); t.mazza@css-mendel.it (T.M.)
⁴ IRCCS Stella Maris Foundation, 56128 Pisa, Italy; r.pasquariello@fsm.unipi.it (R.P.); anna.rubegni@fsm.unipi.it (A.R.); filippo.santorelli@fsm.unipi.it (F.S.); roberta.battini@unipi.it (R.B.)
⁵ Department of Clinical and Experimental Medicine, University of Pisa, 56128 Pisa, Italy
* Correspondence: enzamaría.valente@unipv.it

Featured Application: The combination of bilateral striatal hyperintensities and cerebellar atrophy in patients with progressive encephalopathies represents a “red flag” for PMPCA mutations and may help address the diagnosis and improve management and counseling.

Abstract: Background: Peptidase mitochondrial processing alpha (PMPCA) biallelic mutations cause a spectrum of disorders ranging from severe progressive multisystemic mitochondrial encephalopathy to a milder non-progressive cerebellar ataxia with or without intellectual disability. Recently, we and others described an intermediate phenotype in two unrelated patients. Methods: We report a second Italian patient carrying novel PMPCA variants (p.Trp278Leu; p.Arg362Gly). Molecular modeling, dynamics simulation, RT-qPCR, and Western blotting were performed to predict the pathogenic impact of variants in the two Italian patients and attempt genotype-phenotype correlates. Results: In line with the two patients with intermediate phenotypes, our case presented global psychomotor delay with regression, intellectual disability, spastic-ataxic gait, and hyperkinetic movements, with cerebellar atrophy and bilateral striatal hyperintensities. However, blood lactate, muscle biopsy, and MRI spectroscopy were normal. PMPCA protein levels were significantly higher than controls despite normal cDNA levels. Dynamics simulation of several PMPCA missense variants showed a variable impact on the flexibility of the glycine rich loop and, for some cases, on the overall protein stability, without clear genotype-phenotype correlates. Conclusion: We confirm the expansion of PMPCA phenotypic spectrum including an intermediate phenotype of progressive encephalopathy without systemic involvement. The association of cerebellar atrophy with “Leigh-like” striatal hyperintensities may represent a “red flag” for this condition.

Keywords: SCAR2; PMPCA; non progressive cerebellar atrophy; mitochondrial encephalopathy; striatal hyperintensity; α -MPP; frataxin



Citation: Serpieri, V.; Biagini, T.; Mazzotta, C.; Pasquariello, R.; Rubegni, A.; Santorelli, F.; Ongari, G.; Cerri, S.; Mazza, T.; Battini, R.; et al. Phenotypic Definition and Genotype-Phenotype Correlates in PMPCA-Related Disease. *Appl. Sci.* **2021**, *11*, 748. <https://doi.org/10.3390/app11020748>

Received: 17 December 2020

Accepted: 11 January 2021

Published: 14 January 2021

Publisher’s Note: MDPI stays neutral with regard to jurisdictional claims in published maps and institutional affiliations.



Copyright: © 2021 by the authors. Licensee MDPI, Basel, Switzerland. This article is an open access article distributed under the terms and conditions of the Creative Commons Attribution (CC BY) license (<https://creativecommons.org/licenses/by/4.0/>).

1. Introduction

The advent of next generation sequencing techniques has greatly eased the identification of novel genes causative of Mendelian disorders while disclosing a previously unsuspected degree of pleiotropy. Indeed, variants in the same gene are often found to cause a broad spectrum of phenotypes, with variable severity and clinical presentation, possibly encompassing distinct disorders. The reasons underlying such pleiotropy are still mostly unknown, and genotype-phenotype correlates remain scarce.

One such example is the peptidase mitochondrial processing alpha (*PMPCA*) gene, encoding the alpha subunit of mitochondrial processing peptidase (α -MPP), a heterodimeric enzyme responsible for the cleavage of nuclear-encoded mitochondrial precursor proteins after import in mitochondria. α -MPP is characterized by the glycine-rich loop (GRL, residues 345–358), a key structural element of MPP that recognizes and binds the precursor protein substrate toward the active site [1–3].

Biallelic pathogenic missense variants in the *PMPCA* gene have been associated with two distinct conditions. The first is an early onset, non-progressive cerebellar ataxia (NPCA) with or without developmental delay and intellectual disability, termed “recessive spinocerebellar ataxia type 2” (SCAR2), which should be kept distinct from SCA2 (spinocerebellar ataxia type 2), an autosomal dominant, adult-onset spinocerebellar ataxia due to a pathological trinucleotide expansion in the ataxin 2 gene. Nineteen patients from five families have been reported, all presenting a typical pattern of non-progressive cerebellar atrophy at brain imaging. Muscle biopsy was normal, although mitochondrial complexes activity was mildly decreased in some cases [4,5]. Patients from three families were homozygous for the p.Ala377Thr variant, the proband in the fourth family was compound heterozygous for the p.Ser96Leu and p.Gly515Arg variants, while the two affected siblings in the fifth family were homozygous for the p.Val256Met variant.

The second condition is a much more severe progressive mitochondrial encephalopathy, presenting with profound developmental delay, ptosis, ophthalmoplegia, weakness, respiratory insufficiency, blindness, cardiomyopathy, liver failure, and lactic acidemia, reported in two siblings who were compound heterozygous for the recurrent p.Ala377Thr and the novel p.Gly356Ser variant. Brain MRI showed diffuse cerebellar and cerebral atrophy, with a lactate peak at MRI spectroscopy, while muscle biopsy demonstrated enlarged, structurally abnormal mitochondria [3].

Recently, we reported a 7-year-old Italian boy (here termed “Ita-2”) homozygous for a novel *PMPCA* missense variant (p.Arg185Trp), presenting a phenotype of intermediate severity characterized by a progressive encephalopathy without extra-neurological involvement. He had psychomotor delay with regression, intellectual disability, a spastic-ataxic gait, and upper limb dystonia. Mitochondrial involvement was demonstrated by a slight elevation of blood lactate, as well as multiple defects of oxidative metabolism and signs of mitochondrial proliferation at muscle biopsy. In addition to cerebellar atrophy, brain MRI showed bilateral symmetric hyperintensity in the striatum, resembling the pattern of bilateral striatal necrosis typical of Leigh syndrome [6]. A similar presentation was very recently reported in a 15-year-old Japanese patient [7].

Here, we further define the *PMPCA*-associated phenotypic spectrum by reporting a 12-year-old Italian girl with a similar “intermediate” phenotype of progressive encephalopathy lacking extra-neurological signs. Although she did not present biochemical signs of mitochondrial involvement, brain imaging showed the same peculiar combination of cerebellar atrophy and bilateral “Leigh-like” striatal hyperintensity, suggesting this neuroradiological feature may represent a hallmark of the *PMPCA*-associated intermediate phenotype.

2. Patients and Methods

2.1. Genetic Analysis

The proband (NG2880) was ascertained through a research project aimed at detecting the underlying genetic defect in a large cohort of patients with pediatric ataxias. The local ethics committee approved the project, and parents signed a written informed consent. Clinical, laboratory, and imaging data were obtained through routine diagnostic examinations. Parents consented to a skin biopsy for research purposes; cultured fibroblasts of the Ita-2 patient were already available.

Clinical exome sequencing was performed using SureSelect QXT Focused Exome (Agilent, Santa Clara, CA, United States) and run on NetSeq500 sequencer (Illumina, San Diego, CA, United States), as per manufacturer’s protocol. Bioinformatic analysis was carried out as reported [8]. Variants were filtered based on effect (retained only variants

affecting protein sequence or splicing), frequency (minor allele frequency <1% in general population), and quality (reads >10 and positive quality passive filter). Retained variants were classified according to American college of Medical Genetics (ACMG) criteria, using Varsome [9]. Candidate variants were confirmed by Sanger sequencing using the Big Dye Terminator chemistry (Applied Biosystems, Foster City, CA, USA).

2.2. Cell Cultures

Skin-derived primary fibroblasts from both Italian patients (NG2880 and Ita-2) and three healthy controls were cultured in Roswell Park Memorial Institute Medium (RPMI 1640 w/o L-glutamine) (Carlo Erba Reagents, Cornaredo, Italy) supplemented with inactivated 20% fetal bovine serum (FBS), 1% L-glutamine 200 mM, and 1% penicillin/streptomycin 100X (Euroclone, Pero, Italy), at 5% CO₂ and 37 °C. The medium was replaced three times per week until fibroblasts reached confluence. Fibroblasts were detached with trypsin (Trypsin-EDTA with Phenol Red, Euroclone) and either replated, pelleted or cryopreserved.

2.3. Real-Time PCR Analysis

Total RNA was extracted from fibroblasts with the combination of Trizol and column kit activity (Direct-zol™ RNA MiniPrep Plus w/Zymo-Spin™ IICG Columns, Euroclone). A total amount of 1000 ng was reverse transcribed using High-Capacity cDNA Reverse Transcription Kit (Thermo Fisher Scientific, Waltham, MA, USA).

After cDNA synthesis, 24 ng for each sample (1.6 ng/μL), together with 14.4 μL PowerUp™ SYBR™ Green Master Mix (Applied Biosystems) and 0.6 μL primer mix (40 μM each) were loaded in duplicate into hard-shell 96-well PCR plates and run on CFX Connect detection system (Biorad, Hercules, CA, United States). Primer sequences are available upon request. Data were analyzed with the $\Delta\Delta CT$ method and glyceraldehyde-3-phosphate dehydrogenase (GAPDH) was used as internal control. Statistical analysis was performed using two-tailed Student's *t*-test.

2.4. Cell Extracts and Western Blot

Protein lysates were obtained by resuspending fibroblast pellets in 100 μL of CellLytic lysis buffer containing protease and phosphatase inhibitors (Sigma-Aldrich, St. Louis, MI, United States). Samples were kept on ice and placed on a shaker for 30 min, then centrifuged 16,000× *g* for 20 min at 4 °C. Proteins quantification was performed by the bicinchoninic acid method (Sigma). The absorbance was measured at 562 nm wavelength on CLARIOstar^{Plus} microplate reader (BMG LABTECH, Ortenberg, Germany).

Protein samples (20 μg) were resolved by electrophoretic run on a Mini-Protean® TGX™ gel and transferred to nitrocellulose membranes through the Trans-Blot Turbo Transfer System (Biorad). Membranes were blocked with a commercial buffer (Li-Cor Biosciences, Lincoln, NE, USA) and immunoblotted with primary (anti PMPCA, 1:500—Santa Cruz Biotechnology, Dallas, TX, United States; anti β-actin, 1:10,000—St. John's Laboratory, London, UK) and secondary antibodies (IRDye 800 donkey anti goat and IRDye 700 donkey anti-mouse, Li-Cor). Blots were imaged with the Odyssey System (Li-Cor) and the fluorescent signal obtained from each protein was normalized with the corresponding β-actin signal.

Data were expressed as percentage compared to the average of control samples, in each membrane. Statistical analysis was performed using two-tailed Student's *t*-test.

2.5. Molecular Modeling and Dynamics Simulation

Atomic coordinates of the human MPP heterodimer (Mitochondrial Processing Peptidase alpha and beta subunits, PMPCA and PMPCB) were obtained through homology modeling with SwissModel [10] using the Yeast Mitochondrial Processing Peptidase structure (PDB id: 1hr6, chain A, sequence identity = ~36%) as a template for PMPCA and the Bovine Cytochrome bc1 complex subunit 1 (PDB id: 5okd, chain A, sequence identity = ~57%) as a template for PMPCB. Then, the PMPCA (residues 64 to 510) and PMPCB

(residues 45 to 488) models were superimposed to the Yeast Mitochondrial Processing Peptidase structure using the MatchMaker extension of UCSF Chimera to recreate the heterodimer. The wild-type structure of the heterodimer was mutated in silico to introduce the following missense variants: p.Ala377Thr, p.Gly356Ser, p.Arg185Trp, p.Trp278Leu, p.Gly356Ser, and p.Val256Met.

These were simulated by the Gaussian accelerated Molecular Dynamics (GaMD) technique [11]. A time step of 2 femtoseconds (fs) was set, and then 250 nanoseconds (ns) of GaMD simulations were performed. Each system was simulated three times using AMBER 18 [12] running on 1 NVIDIA Quadro P6000 and 3 NVIDIA RTX 2080Ti [13]. Root-mean-square deviation (RMSD), to measure the average distance between the positions of the C α atomic coordinates and those of the reference X-ray structure over time, and dynamic cross-correlation maps (DCCMs), to study the long-range interactions between all pairs of atoms, were computed [14].

3. Results

3.1. Case Report and Genetic Results

The proband (NG2880), a 12-year-old girl, was born to healthy Italian unrelated parents; an older brother is healthy. She presented an early-onset progressive encephalopathy characterized by global developmental delay with psychomotor regression since age 18 months, intellectual disability, and microcephaly. Her neuromotor phenotype is complex, combining ataxic features, pyramidal signs, and a major hyperkinetic movement disorder with choreic, ballistic, and dystonic components. At age 9 years, she started manifesting seizures, which are only partially controlled by pharmacological treatment with Levetiracetam.

Brain MRI at 18 months of life only showed cerebellar atrophy. A later MRI exam at age 4 years confirmed the non-progressive cerebellar atrophy but disclosed thinning of the corpus callosum, mild cerebral atrophy, and bilateral T2-hyperintensity and hypotrophy of both putamen and caudate (Figure 1A). Blood lactate and muscle biopsy were normal, and there were no lactate peaks at MRI spectroscopy, ruling out a mitochondrial encephalopathy.

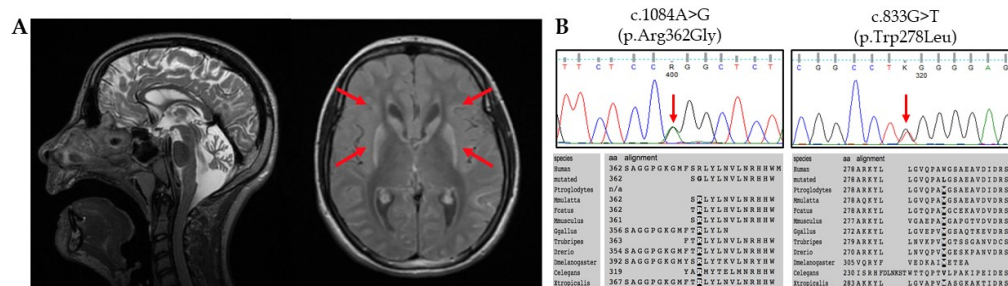


Figure 1. (A) Brain MRI of patient NG2880. Sagittal T2-weighted image (left panel) showing global cerebellar atrophy and thin corpus callosum; axial T1-weighted image (right panel) showing hyperintensity and hypotrophy of caudate nuclei and putamen (red arrows). (B) Electropherograms showing the two identified variants and conservation across species.

Given the phenotypic complexity and the difficulty to select a specific gene panel, the patient was addressed to a clinical exome analysis, which identified two novel heterozygous missense variants (c.833G > A, p.Trp278Leu; c.1084A > G, p.Arg362Gly) in the *PMPCA* gene, both affecting highly conserved residues (Figure 1B). Variants were both classified as likely pathogenic according to ACMG guidelines. They are absent in public databases and consistently predicted as damaging by several prediction softwares, such as Polyphen2, SIFT, and Mutation Taster.

3.2. Functional Assays

To assess the impact of missense mutations associated with *PMPCA* intermediate phenotype on protein expression, we compared Western blotting of the expression levels of α -MPP in fibroblasts from the two Italian patients versus controls. Interestingly, we observed unexpected differences between the two patients: while protein levels of Ita-2 patient were halved compared to controls, patient NG2880 showed an inverted trend, with significantly higher levels than controls (Figure 2).

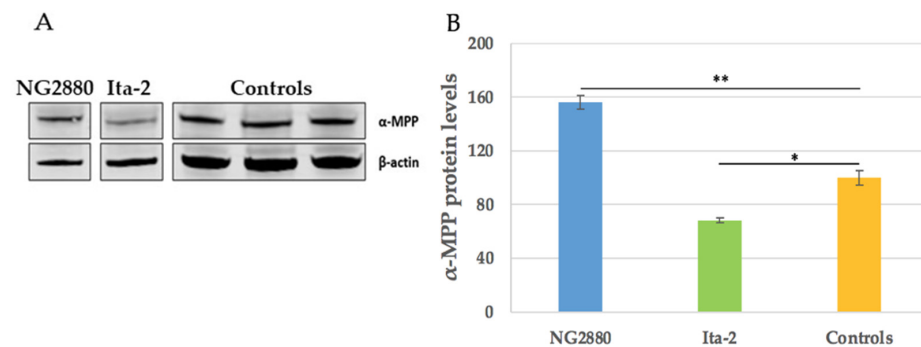


Figure 2. Protein levels of alpha subunit of mitochondrial processing peptidase (α -MPP) in the two Italian patients with intermediate phenotypes versus controls (average of three healthy subjects). (A) Representative Western blot of α -MPP and β -actin (as normalizer). (B) Densitometric analysis from three independent experiments. Protein levels in patients are represented as percentage of control (average of three healthy controls) set at 100. Error bars indicate standard error of the mean (SEM). * $p < 0.05$; ** $p < 0.01$.

To check whether the observed variations in protein expression levels could relate to differences in mRNA levels, we next performed qRT-PCR from retrotranscribed cDNA. However, we did not observe any difference at the cDNA level between the two patients and controls (data not shown), suggesting that the observed differences at the protein level could relate to post-translational modifications.

3.3. In Silico Molecular Modeling and Simulation

All *PMPCA* mutations reported to date are missense variants, variably distributed throughout the protein, except for one frameshift variant very recently reported (Figure 3). To attempt performing genotype-phenotype correlates, we performed in silico modeling of a few missense variants detected in patients with severe, intermediate, and mild phenotypes (Figure 4). We compared the behavior of wild type (wt) versus mutant proteins to measure the impact on the protein structure and stability induced by each variant.

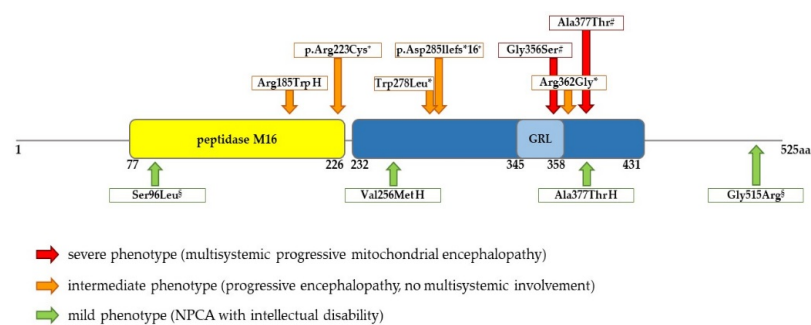


Figure 3. Established peptidase mitochondrial processing alpha (*PMPCA*) domain structure and location of missense mutations previously reported. Mutations identified in homozygous state are indicated with H, while heterozygous mutations identified together in a compound heterozygous state are equally marked (*, #, ^S or +). For each mutation, severity of related phenotype is indicated with a color code.

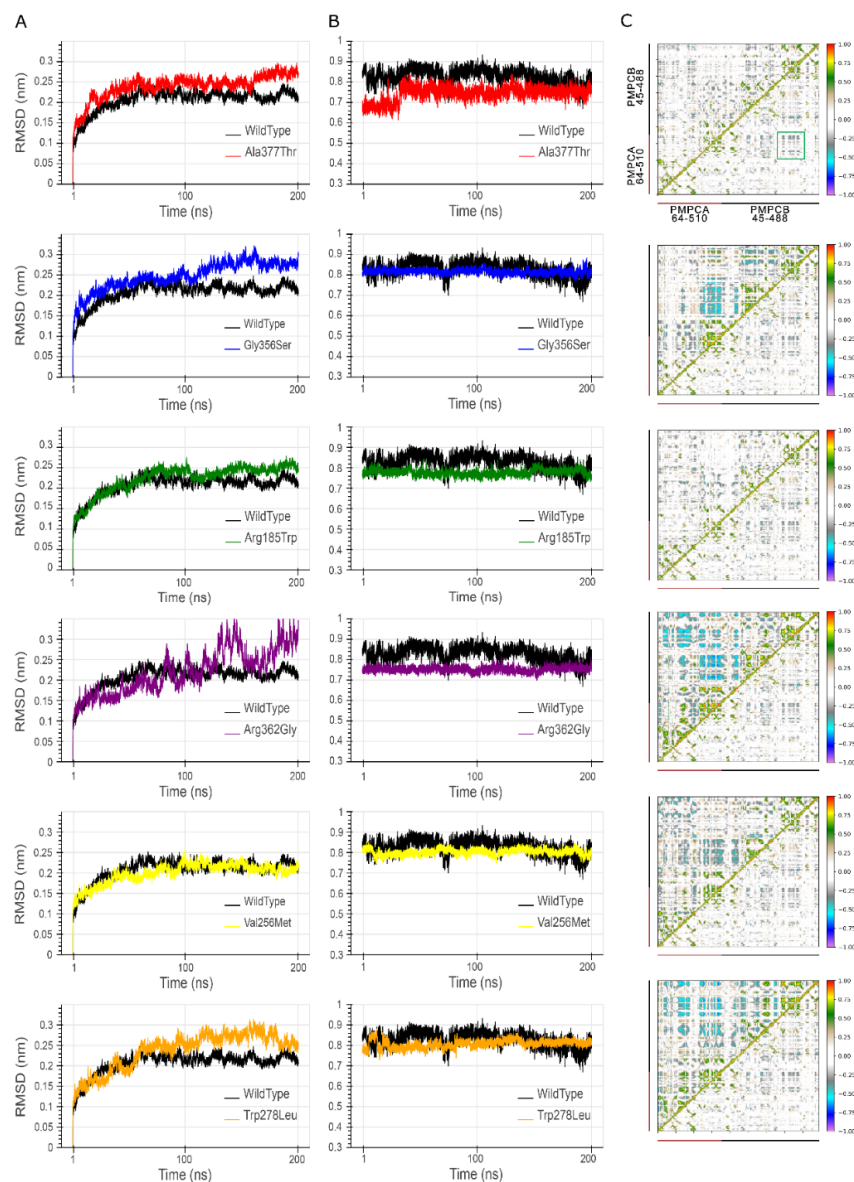


Figure 4. Root-mean-square deviation (RMSD) profiles of the C_{α} atoms of the wild type (wt) (black) and all mutant systems for the whole heterodimer (A) and the glycine-rich loop (B). (C) Dynamic cross-correlation maps (DCCMs) of wt (lower triangular of each matrix) and all PMPCA mutants (upper triangular). Perfect correlations are highlighted in red (direct) or violet (inverse). Green box highlights the wt anticorrelated movements between residues 300 and 400.

The wt heterodimer exhibited increased values of RMSD for the first 50 ns and then reached a plateau, fluctuating in a range of 0.18–0.24 nm, compared with the reference starting structure. All mutants exhibited less stable and higher RMSD values than wt but p.Val256Met, which overlapped the wt profile (Figure 4A). Focusing on the glycine-rich loop, all mutants showed more stable RMSD values than wt (Figure 4B), with p.Arg185Trp, p.Arg362Gly, and p.Ala377Thr being the most dissimilar with ~ 0.1 nm lower RMSD values. Regarding the DCCM profiles, variants p.Val256Met, p.Trp278Leu, p.Gly356Ser, and p.Arg362Gly showed a dramatic increase in all atomic motions (Figure 4C), reflecting an evident gain in the overall mobility compared to the wt system, while p.Arg185Trp and p.Ala377Thr were similar to wt. The regions spanning residues 300–400 of PMPCB and 260–460 of PMPCA (the latter containing the GRL) exhibited anticorrelated movements, which were lost in mutants p.Arg185Trp, p.Val256Met, p.Gly356Ser, and p.Ala377Thr, finally suggesting a decreased flexibility of the glycine-rich region in these mutants.

4. Discussion

An increasing number of genes are progressively associated with a broad spectrum of phenotypes, even encompassing different disorders. In these cases, an accurate mapping of gene-associated phenotypes is mandatory, as it would help the diagnostic lab to select the appropriate gene panels (or virtual gene panels in case of exome sequencing), and therefore increase the diagnostic yield.

Here we contribute to delineate the phenotypic spectrum associated with recessive mutations in the *PMPCA* gene. So far, two well-distinct conditions have been delineated: (1) a severe progressive mitochondrial encephalopathy with multiorgan involvement, characterized by profound psychomotor delay, ptosis, ophthalmoplegia, hypotonia and severe generalized weakness, optic atrophy, cardiomyopathy, liver failure, global brain atrophy, and evidence of mitochondrial involvement (lactic acidemia, lactate peak at MRI spectroscopy, abnormal mitochondria at muscle biopsy); (2) a much milder neurological disorder characterized by non-progressive cerebellar atrophy and NPCA with or without intellectual disability, lacking any obvious mitochondrial sign.

We now confirm the existence of a third *PMPCA*-associated phenotype of intermediate severity, presenting as a progressive encephalopathy with psychomotor regression, intellectual disability, spastic ataxia, and a variable hyperkinetic movement disorder, but without extra-neurological signs of mitochondriopathy. In addition to cerebellar atrophy, patients present a peculiar neuroradiological hallmark, represented by bilateral symmetric T2-weighted hyperintensities of the basal ganglia, resembling those seen in Leigh syndrome. However, it is important to note that our patient lacked obvious signs of mitochondrial involvement (blood lactate, muscle biopsy, and MRI spectroscopy were normal), which instead were present in the first patient. Just before submission of this manuscript, a 15-year-old Japanese girl was reported with a similar phenotype of severe and progressive developmental delay, cerebellar ataxia, and extrapyramidal symptoms. Brain imaging showed cerebellar atrophy and abnormal signal in the basal ganglia, which was interpreted as iron accumulation; however, it is likely that this girl also fell in the “*PMPCA* intermediate phenotype” category highlighted here, characterized by peculiar Leigh-like basal ganglia hyperintensities in association to cerebellar atrophy [7].

All pathogenic variants in the *PMPCA* gene are missense variants variably distributed throughout the protein (Figure 3) that are highly conserved among vertebrates and consistently predicted as damaging by prediction software. Previous studies have attempted to define the functional impact of specific amino acid substitutions on the stability and function of α -MPP protein and correlate these effects with the observed phenotype. In particular, mutant α -MPP was found to impair processing of the mitochondrial protein frataxin, causing an accumulation of the intermediate forms and reduced levels of the processed protein [15]. Interestingly, abnormal frataxin processing was demonstrated in lymphoblasts and/or fibroblasts from patients presenting either with the severe (compound heterozygous for p.Ala377Thr and p.Gly356Ser variants) or the mild phenotype (homozygous for p.Ala377Ser or for p.Val256Met variants) [3–5]. Moreover, α -MPP levels were measured in lymphoblasts from patients presenting the mild phenotype homozygous for two distinct mutations: while cells with the p.Ala377Thr variant showed significantly reduced levels of α -MPP, these were comparable to controls in cells carrying the p.Val256Met variant [4,5]. Taken together, these findings suggest a loss of function mechanisms underlying *PMPCA* missense variants (as also pointed out by the frameshift mutation recently reported in the Japanese patient) but fail to disclose any specific genotype-phenotype correlates at the functional level. This is further confirmed by our findings on fibroblasts from the two Italian patients with intermediate phenotypes, as we unexpectedly observed opposite trends regarding α -MPP expression levels, which were halved than controls in cells from the patient Ita-2 (homozygous for the p.Arg185Trp variant) but were significantly increased compared to controls in patient NG2880 (compound heterozygous for p.Trp278Leu and p.Arg362Gly variants). Since RNA expression levels were comparable in the two patients and similar to controls, the altered levels of α -MPP are likely related to the variable impact

of missense variants on the protein stability, influencing its physiological turnover within the cell.

To further attempt a dissection of the functional effect of distinct missense variants, we performed molecular modeling of the human MPP heterodimer, and a systematic dynamic simulation of several missense mutants compared to wild type (Figure 4). Such an approach was already proposed by Jobling and collaborators. They suggested that the substitution of a Serine with the bulkier Threonine at position 377, lying in close proximity to the GRL, would interfere with the loop flexibility and, therefore, with the ability to bind substrates stably [4]. Similarly, Joshi and coworkers performed computer modeling for the same p.Ala377Thr and for p.Gly356Ser, which were compound heterozygous in their patients with severe phenotype. Since p.Gly356Ser falls within the GRL, the authors proposed that both mutations would restrict the dynamic movements of the catalytic loop, therefore affecting substrate binding or catalytic activity of the protein [3].

Our widespread dynamic simulations showed that all analyzed mutants could variably impact on the GRL flexibility and some also influenced the overall stability of the entire MPP heterodimer. In particular, the variants p.Arg185Trp, p.Arg362Gly, and p.Ala377Thr exhibited lower RMSD values than the wt for the simulations' entire duration, reflecting an increased rigidity and significant impairment of the GRL mobility. Conversely, the impact of p.Val256Met, p.Trp278Leu, and p.Gly356Ser on the GRL seemed less evident, although flexibility is always lower than wt. However, these three variants (as well as p.Arg362Gly) showed a more relevant impact on the overall stability of the heterodimer, as they induced a strong increase in anticorrelation motions between the two proteins. These data confirm that missense variants of *PMPCA* variably affect either the degree of rigidity of the GRL and/or the global stability of the protein, likely resulting in impaired substrate binding or catalytic activity of the complex. However, our findings argue against the existence of reliable genotype-phenotype correlations, suggesting that the phenotypic manifestations of *PMPCA*-related disease are likely influenced by modifier factors, which remain to be disclosed.

5. Conclusions

In conclusion, we report two novel *PMPCA* missense variants in an Italian patient and confirm the existence of an "intermediate" *PMPCA*-associated phenotype characterized by a progressive encephalopathy without systemic signs of mitochondriopathy. The association of cerebellar atrophy with T2-weighted bilateral striatal hyperintensity may represent a "red flag" for this presentation.

Author Contributions: Conceptualization, V.S. and E.M.V.; investigation, validation, and formal analysis, V.S., C.M., G.O., T.B., T.M., R.P. and A.R.; writing—original draft preparation, V.S., G.O., and T.B.; writing—review and editing, S.C., T.M., R.B., F.S., and E.M.V.; supervision, E.M.V.; project administration, V.S. and E.M.V.; funding acquisition, E.M.V. All authors have read and agreed to the published version of the manuscript.

Funding: This research was funded by Italian Ministry of Health (Ricerca Corrente 2020 and Ricerca Finalizzata grant number NET-2013-02356160) and Pierfranco and Luisa Mariani Foundation (PADAPORT).

Institutional Review Board Statement: The study was conducted according to the guidelines of the Declaration of Helsinki, and approved by the Institutional Review Board (or Ethics Committee) of University of Pavia (protocol code 20180077857 and 12 September 2018).

Informed Consent Statement: Informed consent was obtained from all subjects involved in the study.

Data Availability Statement: No new data were created or analyzed in this study. Data sharing is not applicable to this article.

Acknowledgments: We are grateful to Antonio Otranto for technical support.

Conflicts of Interest: The authors declare no conflict of interest.

References

1. Gakh, O.; Cavadini, P.; Isaya, G. Mitochondrial processing peptidases. *Biochim. Biophys Acta* **2002**, *1592*, 63–77. [[CrossRef](#)]
2. Taylor, A.B.; Smith, B.S.; Kitada, S.; Kojima, K.; Miyaura, H.; Otwinowski, Z.; Ito, A.; Deisenhofer, J. Crystal structures of mitochondrial processing peptidase reveal the mode for specific cleavage of import signal sequences. *Structure* **2001**, *9*, 615–625. [[CrossRef](#)]
3. Joshi, M.; Anselm, I.; Shi, J.; Bale, T.A.; Towne, M.; Schmitz-Abe, K.; Crowley, L.; Giani, F.C.; Kazerounian, S.; Markianos, K.; et al. Mutations in the substrate binding glycine-rich loop of the mitochondrial processing peptidase-alpha protein (PMPCA) cause a severe mitochondrial disease. *Cold Spring Harb. Mol. Case Stud.* **2016**, *2*, a000786. [[CrossRef](#)] [[PubMed](#)]
4. Jobling, R.K.; Assoum, M.; Gakh, O.; Blaser, S.; Raiman, J.A.; Mignot, C.; Roze, E.; Durr, A.; Brice, A.; Levy, N.; et al. PMPCA mutations cause abnormal mitochondrial protein processing in patients with non-progressive cerebellar ataxia. *Brain* **2015**, *138*, 1505–1517. [[CrossRef](#)] [[PubMed](#)]
5. Choquet, K.; Zurita-Rendon, O.; La Piana, R.; Yang, S.; Dicaire, M.J.; Care4Rare Consortium; Boycott, K.M.; Majewski, J.; Shoubbridge, E.A.; Brais, B.; et al. Autosomal recessive cerebellar ataxia caused by a homozygous mutation in PMPCA. *Brain* **2016**, *139*, e19. [[CrossRef](#)] [[PubMed](#)]
6. Rubegni, A.; Pasquariello, R.; Dosi, C.; Astrea, G.; Canapicchi, R.; Santorelli, F.M.; Nesti, C. Teaching NeuroImages: Leigh-like features expand the picture of PMPCA-related disorders. *Neurology* **2019**, *92*, e168–e169. [[CrossRef](#)] [[PubMed](#)]
7. Takahashi, Y.; Kubota, M.; Kosaki, R.; Kosaki, K.; Ishiguro, A. A severe form of autosomal recessive spinocerebellar ataxia associated with novel PMPCA variants. *Brain Dev.* **2020**. [[CrossRef](#)]
8. Ginevrino, M.; Battini, R.; Nuovo, S.; Simonati, A.; Micalizzi, A.; Contaldo, I.; Serpieri, V.; Valente, E.M. A novel IRF2BPL truncating variant is associated with endolysosomal storage. *Mol. Biol. Rep.* **2020**, *47*, 711–714. [[CrossRef](#)]
9. Kopanos, C.; Tsiolkas, V.; Kouris, A.; Chapple, C.E.; Albarca Aguilera, M.; Meyer, R.; Massouras, A. VarSome: The human genomic variant search engine. *Bioinformatics* **2019**, *35*, 1978–1980. [[CrossRef](#)] [[PubMed](#)]
10. Schwede, T.; Kopp, J.; Guex, N.; Peitsch, M.C. SWISS-MODEL: An automated protein homology-modeling server. *Nucleic Acids Res.* **2003**, *31*, 3381–3385. [[CrossRef](#)] [[PubMed](#)]
11. Miao, Y.; Feher, V.A.; McCammon, J.A. Gaussian Accelerated Molecular Dynamics: Unconstrained Enhanced Sampling and Free Energy Calculation. *J Chem Theory Comput.* **2015**, *11*, 3584–3595. [[CrossRef](#)]
12. Peters, M.B.; Yang, Y.; Wang, B.; Füsti-Molnár, L.; Weaver, M.N.; Merz, K.M., Jr. Structural Survey of Zinc Containing Proteins and the Development of the Zinc AMBER Force Field (ZAFF). *J. Chem. Theory Comput.* **2010**, *6*, 2935–2947. [[CrossRef](#)] [[PubMed](#)]
13. Biagini, T.; Petrizzelli, F.; Truglio, M.; Cespa, R.; Barbieri, A.; Capocéfalo, D.; Castellana, S.; Tevy, M.F.; Carella, M.; Mazza, T. Are Gaming-Enabled Graphic Processing Unit Cards Convenient for Molecular Dynamics Simulation? *Evol Bioinform. Online* **2019**, *15*. [[CrossRef](#)] [[PubMed](#)]
14. Biagini, T.; Chillemi, G.; Mazzoccoli, G.; Grottesi, A.; Fusilli, C.; Capocéfalo, D.; Castellana, S.; Vescovi, A.L.; Mazza, T. Molecular dynamics recipes for genome research. *Brief Bioinform.* **2018**, *19*, 853–862. [[CrossRef](#)] [[PubMed](#)]
15. Cavadini, P.; Adamec, J.; Taroni, F.; Gakh, O.; Isaya, G. Two-step processing of human frataxin by mitochondrial processing peptidase. Precursor and intermediate forms are cleaved at different rates. *J. Biol. Chem.* **2000**, *275*, 41469–41475. [[CrossRef](#)]